Postprint of: Pietrenko-Dąbrowska A., Kozieł J., Optimization-Based Robustness Enhancement of Compact Microwave Component Designs with Response Feature Regression Surrogates, KNOWLEDGE-BASED SYSTEMS (2022), 108161, DOI: 10.1016/j.knosys.2022.108161

Optimization-Based Robustness Enhancement of Compact Microwave Component Designs with Response Feature Regression Surrogates

Anna Pietrenko-Dabrowska[1] ,Slawomir Koziel[2,1]

[1] Faculty of Electronics, Telecommunications and Informatics, Gdansk University of Technology, 80-233 Gdansk, Poland, anna.dabrowska@pg.edu.pl

[2] Engineering Optimization & Modeling Center, Reykjavik University, 102 Reykjavik, Iceland, koziel@ru.is

Keywords: Microwave design, miniaturized circuits, uncertainty quantification, robust design, tolerance optimization, feature-based models, knowledge-based surrogates.

Abstract

The ability to evaluate the effects of fabrication tolerances and other types of uncertainties is a critical part of microwave design process. Improving the immunity of the device to parameter deviations is equally important, especially when the performance specifications are stringent and can barely be met even assuming a perfect manufacturing process. In the case of modern miniaturized microwave components of complex topologies, it is of paramount importance to carry out tolerance-aware design at the highest available accuracy level (i.e., with the use of full-wave electromagnetic (EM) simulations). Although reliable, EM-driven tolerance-aware design is extremely costly if conventional techniques are to be applied (e.g., Monte Carlo simulation). To overcome this setback, this paper proposes a simple and computationally efficient algorithm for robustness enhancement of compact microwave component designs. The objective is to increase the allowed deviations of geometry parameter values (described using the coefficients of an underlying probability distributions, e.g., the variance) so that the prescribed performance specifications are still fulfilled. The presented approach incorporates knowledge-based surrogate models, constructed using the characteristic points (response features) of EM-simulated system outputs, and utilized for low-cost prediction of the fabrication yield. The parameter vector of the microwave circuit of interest is adjusted within the trust-region (TR) framework to identify the maximum levels of deviations still ensuring 100-percent yield. The employment of TR also permits the adaptive control of design relocation and ensures convergence of the optimization process. Numerical verification of the presented methodology is carried out using three miniaturized microstrip circuits, including two equal-split couplers and a wideband filter. The major finding is that incorporating knowledge-based feature surrogates allows for achieving a significant improvement of the acceptable input tolerance levels (nearly two fold on the average) at a remarkably low cost of few dozen EM simulations.

1. Introduction

The fulfillment of stringent performance specifications imposed on microwave components and systems, including wideband [1] and multi-band operation [2], tunability [3], specific demands pertinent to emerging application areas (5G [4], internet of things [5], wearable devices [6], etc.), and—more and more often—compact size [7]-[10], has been increasingly difficult. In general, it requires the development of topologically complex structures, the dimensions of which have to be meticulously tuned to ensure the best possible values of the operating parameters (bandwidth, phase response, power split levels, etc.). In most cases, the designs are optimized in the nominal sense [11]-[13], that is, by neglecting possible fabrication tolerances and other uncertainties (e.g., imprecise knowledge of the substrate permittivity), including operating conditions (temperature, different signal power levels, etc.). Needless to say, these may affect the system characteristics, often leading to a violation of the performance requirements. Unfortunately, parameter deviations are unavoidable due to inherently limited manufacturing process accuracy, whereas reducing the deviations normally increases the fabrication expenses. Consequently, the ability to quantify the uncertainties and mitigate their effects is of fundamental importance when it comes to ensuring design robustness [14]. In practice, this is addressed by maximizing a suitably chosen statistical performance figures, e.g., the yield [15]. An alternative approach is to increase the maximum level of parameter deviations that still ensure satisfaction of the specs (e.g., the improvement of the maximum input tolerance hypervolume, MITH [16]).

Statistical analysis of microwave components is a computationally expensive task when directly conducted using full-wave electromagnetic (EM) simulation models. For example, the primary analysis procedure, Monte Carlo (MC) simulation [17], normally requires many hundreds of system evaluations due to its slow convergence. On the other hand, the employment of EM models is often imperative, especially for miniaturized components where considerable

cross-coupling effects virtually rule out utilization of simpler models (e.g., equivalent networks [18]). Simplification of the task is one way to accelerate the process, which can be realized by performing a worst-case analysis [19], [20]. However, it typically results in an overly pessimistic estimation of the tolerance effects. Nowadays, the most popular approach to practical EM-based uncertainty quantification (UQ) is the incorporation of surrogate modeling techniques [21], [22]. These may belong to two groups: data-driven (kriging [23], neural networks [24], Gaussian process regression [25], polynomial chaos expansion, PCE [26], [27]), and physics-based (e.g., space mapping [28]). The major advantage of surrogate-assisted approach is a possibly dramatic acceleration of all sorts of UQ procedures, including yield estimation. When using PCE, some of the figures of merit, e.g., the statistical moments of the system outputs, can be evaluated directly from the expansion coefficients without the necessity of running MC. Yet, conventional modeling techniques are severely limited in terms of parameter space dimensionality but also parameter ranges (both being a consequence of high nonlinearity of microwave component characteristics). Available mitigation methods include hybrid surrogates (e.g., PC kriging [29]), dimensionality reduction (e.g., principal component analysis, PCA [30]), model order reduction [31], utilization of variable-fidelity EM simulations (co-kriging [32], two-stage GPR [33], space mapping [34]), and, recently, modeling with domain confinement [35], [36].

Although manufacturing tolerances are unavoidable, the robustness of microwave component designs can be improved by proper tuning of the circuit parameters. The respective procedures are referred to as tolerance-aware design, yield-driven design or design centering [37]-[39]. As mentioned before, in many cases (especially in the case of minimax-type of design specifications), the merit function of choice is the yield. Other options include maximization of maximum parameter deviations that do not lead to a violation of the specs, or allocating the design as much in the interior of the feasible space as possible (geometrical design centering

[40]). The tolerances, due to their stochastic nature, are modeled using suitable probability density functions, typically Gaussian with zero mean and a variance (or covariance matrix) specific to a given manufacturing process, or uniform with (also process-specific) maximum deviation. Just as in the case of UQ, statistical optimization is a CPU-heavy task when conducted at the level of EM simulation models, and the primary workaround is the utilization of surrogate modeling methods [41]-[43]. However, robust design is considerably more challenging due to the larger expected design relocation, which implies that the underlying surrogate model should be valid over broader ranges of the circuit parameters. The metamodel can be constructed using machine learning approaches [44], e.g., by adding infill samples in the regions to be explored during the optimization process [45]. Another method is sequential approximate optimization, SAO [46], with the surrogate only rendered in the vicinity of the current design, and the domain moved along the optimization path. Yet another approach is to employ a response feature technique [47], where the surrogate model is representing selected characteristic (feature) points of the circuit outputs rather than the entire frequency responses, which leads to 'flattening' the functional landscape to be modeled while being sufficient to account for performance specifications [48]. Additional benefits can be achieved by means of performance-driven modeling [49], which capitalizes on restricting the volume of the surrogate model domain without reducing it along important directions (i.e., corresponding to the maximum response modifications) [36].

In this work, we propose a technique for low-cost robustness improvement of compact microwave components. It is oriented towards maximization of input tolerances for which the perfect (100-percent) fabrication yield is still ensured and it utilizes problem-specific knowledge in the form of the response features extracted from the gathered data, i.e., frequency characteristics of the device under design. Feature-based surrogates are employed to carry out yield estimation in a computationally efficient manner, whereas the search is executed iteratively and adopts the trust-region concept to permit a control over design relocation during

the optimization process, and to guarantee its convergence. The presented methodology is validated using several examples of microstrip circuits, including two broadband filters and a miniaturized branch-line coupler. In all cases, independent Gaussian probability distribution is chosen to represent the parameter deviations. The input tolerance level—measured using the distribution variance—is improved by a factor of 1.6, 1.5, and 1.8, for the first, second, and third circuit, respectively. The average computational cost of the robustness enhancement process is low and corresponds to only seventy EM circuit simulations. The result reliability, in particular, the predictive power of the feature-based surrogates, has been verified through EM-based Monte Carlo simulations at the nominal and the robust designs.

The major contributions of the paper include: (i) the development of a novel algorithm for simulation-driven tolerance optimization of microwave components that ensures perfect fabrication yield by direct maximization of the input tolerance levels, (ii) ensuring cost-effectiveness of the yield estimation process through the employment of the problem-specific knowledge encoded in the form of feature-based surrogates, (iii) inducing convergence of the tolerance optimization procedure by embedding it in the the trust-region (TR) local search routine, (iv) definition of a performance metric that ensures inexpensive evaluation of the candidate designs yielded by the TR algorithm, (v) establishing the parameter deviation values that do not lead to violation of the design requirements at the cost of a few dozens of EM analyses of the respective circuits.

The paper is organized as follows: Section 2 introduces the proposed algorithm for robustness enhancement of microwave devices, preceded by formulation of the design task, as well as recollection of response features technology. Section 3 delineates the verification case studies, provides the results of the numerical verification of the introduced algorithm, along with their discussion. Section 4 summarizes the research findings and concludes the paper.

2. Robustness Enhancement by Means of Response Feature Surrogates

The purpose of this section is to formulate the proposed procedure for robustness improvement of compact microwave components. The design problem and objectives are stated in Section 2.1. Section 2.2 recalls the concept of response features along with the definition of the knowledge-based surrogate set up at the level of the response features. Section 2.3 defines the objective function and its evaluation procedure. The entire tolerance optimization framework is summarized in Section 2.4. The numerical verification of the procedure will be provided in Section 3.

Table 1. Robustness enhancement with feature-based surrogates: Notation

Purpose	Description	Notation
General	Parameter vector of the circuit	$\boldsymbol{x} = [x_1 \ \ldots \ x_n]^T$
	Frequency	f
Device response	Scattering parameters of microwave circuits	S_{j1}, $j = 1, \ldots, 4$
	Operating frequencies	$f_{0.k}$, $k = 1, \ldots, N$
	Lower, upper frequencies of the kth operating band	$f_{l.k}$, $f_{R.k}$
	Target power split	S_k
	Power split error	D_k
	Acceptance threshold for S_{11} and S_{41}	$S_{\max}$
Tolerance optimization	Nominal design	$\boldsymbol{x}^{(0)}$
	Fabrication yield	Y
	Objective function	U_Y
	Probability density function describing parameter deviations	p
	Variance of Gaussian probability distribution	σ
	Parameter perturbations	d
	Feasible space	X_f
	Random observables	$x_{r,j}$, $j = 1, \ldots, N_r$
Response features	Response features vector	$\boldsymbol{P}(\boldsymbol{x}) = [p_1 \ \ldots \ p_{Np}]^T$
	Frequency coordinate of the feature point	f_i, $i = 1, \ldots, N_p$
	Level coordinate of the feature point	l_i, $i = 1, \ldots, N_p$
Trust-region algorithm	Trust region size	$\boldsymbol{\delta}^{i)}$
	Gain ratio	r
	Termination threshold	ε

2.1. Robustness Enhancement through Input Tolerance Optimization

This section discusses formulation of the nominal design task for exemplary microwave components, definition of statistical performance metrics utilized throughout the paper, as well as the formulation of the robustness enhancement problem.

2.1.1. Performance Specifications and Nominal Design

In order to discuss the robustness enhancement task, we first need to quantify the performance of the microwave circuit at hand. In particular, we need a rigorous formulation of the design specifications, which is specific to a particular class of components. Below, we consider two examples, a microwave coupler, and a bandpass filter. In both cases, $\boldsymbol{x} = [x_1 \ldots x_n]^T$ will stand for a vector of adjustable parameters, whereas f will denote the frequency. In order to facilitate the reading, the notation used henceforth has been highlighted in Table 1.

Multi-band coupler. We formulate the specifications for a multi-band coupler, where $f_{L.k}$ and $f_{R.k}$ denote the lower and upper frequencies determining the kth operating band, $k = 1, \ldots, N$, whereas D_k are maximum power split errors at the operating frequency $f_{0.k} = [f_{R.k} + f_{L.k}]/2$, with S_k being the respective target power split ratio. The circuit satisfies the specifications at the design $\boldsymbol{x}$ if

$$\max\left\{ f \in \bigcup_{k=1}^{N} [f_{L.k}, f_{R.k}] : |S_{11}(\boldsymbol{x}, f)| \right\} \le S_{\max} \tag{1}$$

$$\max\left\{ f \in \bigcup_{k=1}^{N} [f_{L.k}, f_{R.k}] : |S_{41}(\boldsymbol{x}, f)| \right\} \le S_{\max} \tag{2}$$

and

$$\left| |S_{31}(\boldsymbol{x}, f_{0.k})| - |S_{21}(\boldsymbol{x}, f_{0.k})| - S_k \right| \le D_k \qquad k = 1, \ldots, N \tag{3}$$

The acceptance threshold $S_{\max}$ for the matching and isolation characteristics is decided upon by the user, typically, we have $S_{\max} = -20$ dB. Satisfaction of (1)-(3) is equivalent to the circuit featuring a sufficient bandwidth (at the level $S_{\max}$) and realizing a required power split within the assumed tolerance D_k, simultaneously at all operating frequencies.

Bandpass filter. For simplicity, we only consider performance specifications imposed on the reflection response of the filter. Let f_L and f_R be the frequencies determining the intended operating bandwidth, and $S_{\max}$ be the maximum allowed in-band reflection level. The circuit satisfies the specifications at the design $\boldsymbol{x}$ if

$$\max\left\{ f \in \left[f_L, f_R \right] : |S_{11}(\boldsymbol{x}, f)| \right\} \leq S_{\max} \tag{4}$$

In practice, additional requirements are often imposed on both the reflection and transmission response (e.g., maximum in-band ripple level [50], etc.), which is omitted here for the sake of clarity.

In this work, the nominal design, denoted as $\boldsymbol{x}^{(0)}$, will be understood as the one that does not take into account any fabrication tolerances. Typically, it is obtained in a minimax sense using the objective function corresponding to conditions (1)-(3) or (4). For example, in the case of a coupler, we aim at improving the circuit matching $|S_{11}|$ and isolation $|S_{41}|$ within the frequency range or operation, and to maintain the required power split S. In particular, we have

$$\boldsymbol{x}^{(0)} = \arg\min_{\boldsymbol{x}} \left\{ \max\left\{ f \in \bigcup\nolimits_{k=1}^{N} \left[f_{L.k}, f_{R.k} \right] : \max\{ |S_{11}(\boldsymbol{x}, f)|, |S_{41}(\boldsymbol{x}, f)| \} \right\} \right\} \tag{5}$$

which is subject to the equality constraints

$$|S_{31}(\boldsymbol{x}, f_{0.k})| - |S_{21}(\boldsymbol{x}, f_{0.k})| = S_k \qquad k = 1, \ldots, N \tag{6}$$

As the constraints (6) are expensive to evaluate (i.e., extracted from EM-simulated circuit outputs), they are best handled using penalty functions [51]. In the case of a bandpass filter (cf. (4)), the nominal design may be obtained as

$$\boldsymbol{x}^{(0)} = \arg\min_{\boldsymbol{x}} \left\{ \max\left\{ f \in \left[f_L, f_R \right] : |S_{11}(\boldsymbol{x}, f)| \right\} \right\} \tag{7}$$

2.1.2. Fabrication Yield

The primary statistical performance metric utilized in high-frequency design is yield [52]. It is more suitable than, e.g., statistical moments of the system output (e.g., the variance), because the microwave circuit responses are normally vector-valued, whereas design

specifications are often formulated in a minimax form (cf. Section 2.1.1). Furthermore, it explicitly quantifies the likelihood of the design satisfying the specs under the assumed manufacturing tolerances. The yield Y is defined as

$$Y(\boldsymbol{x}^{(0)}) = \int_{X_f} p(\boldsymbol{x}, \boldsymbol{x}^{(0)}) d\boldsymbol{x} \tag{8}$$

where $p(\boldsymbol{x}, \boldsymbol{x}^{(0)})$ is a joint probability density function that describes statistical variations of the design $\boldsymbol{x}$ w.r.t. the nominal design $\boldsymbol{x}^{(0)}$; X_f in (8) denotes the feasible space, i.e., the set containing designs satisfying the given performance requirements (e.g., (1)-(3) for a coupler, or (4) for a filter).

In practice, an explicit integration of the density function $p(\cdot)$ is hardly possible because the feasible space is not explicitly available. Instead, Monte Carlo (MC) simulation is often used, which essentially corresponds to numerical integration of (8). The yield Y is obtained as

$$Y(\boldsymbol{x}^{(0)}) = N_r^{-1} \sum_{k=1}^{N_r} H(\boldsymbol{x}^{(k)}) \tag{9}$$

In (9), $\boldsymbol{x}^{(k)}$, $k = 1, \ldots, N_r$, are random vectors of the form $\boldsymbol{x}^{(k)} = \boldsymbol{x}^{(0)} + d\boldsymbol{x}^{(k)}$, where the deviations $d\boldsymbol{x}^{(k)}$ are generated according to the probability density function $p(\cdot)$. Whereas the function $H(\boldsymbol{x})$ is defined to take the value of 1 if the design specifications are met, and zero otherwise.

In general, the function p depends on the fabrication process as well as correlations between the geometry parameters. In the numerical experiments presented in Section 3, it is assumed that parameter deviations follow independent Gaussian distributions with zero mean and a variance σ. The MC procedure is slowly convergent, i.e., reliable estimation of the yield requires many hundreds or even thousands of system evaluations. Consequently, it incurs considerable computational expenses when carried out directly using EM simulation tools.

2.1.3. Robustness Enhancement Problem Formulation

Perhaps the most popular approach to statistical design of high-frequency components is maximization of yield under specific assumptions concerning manufacturing/material

uncertainties [14], [15], [21], [26], [30], [34]. Therein, the design task is posed as

$$\boldsymbol{x}^* = \arg\min_{\boldsymbol{x}}\{-Y(\boldsymbol{x})\} \tag{10}$$

Practical methods for solving (10) are largely based on surrogate modelling techniques, which is often imperative given a high computational cost of massive EM analyses involved in the process.

The robustness improvement problem can also be formulated from the perspective of input tolerances, which is more insightful in certain situations, especially when the manufacturing process has not yet been selected, or the designer seeks to identify the maximum values of parameter deviations that can be tolerated by the device without violating the performance specifications (cf. maximum input tolerance hypervolume improvement [16]). This is the approach adopted here. In particular, we aim at maximizing the allowable deviations of the circuit geometry parameters for which the yield is still equal to one (i.e., hundred percent). For simplicity, we assume a single parameter governing the tolerance levels, i.e., the variance σ of independent Gaussian probability distributions describing the parameter deviations. The robustness enhancement task is formulated as

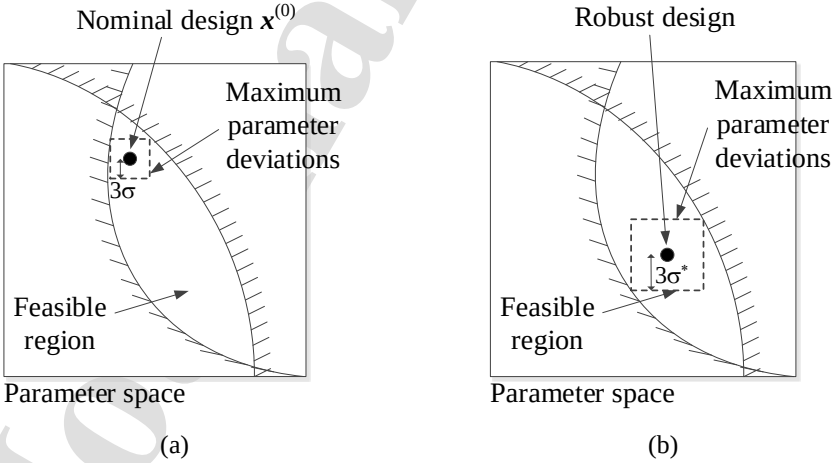

Fig. 1. Robustness enhancement concept: (a) nominal design $\boldsymbol{x}^{(0)}$ and the dashed-line-marked region corresponding to the maximum values of parameter deviations that ensure perfect (100-percent) yield; here, assuming independent Gaussian distributions with a joint variance σ; (b) robust design, featuring enlarged maximum parameter deviations. The nominal objective function value (cf. (5) or (7)) is typically worse at the robust design than at $\boldsymbol{x}^{(0)}$.

$$\boldsymbol{x}^* = \arg\min_{\boldsymbol{x}} U_Y(\boldsymbol{x}) \tag{11}$$

with the objective function U_Y therein defined as

$$U_Y(\boldsymbol{x}) = \arg\max_{\sigma} \{Y(\boldsymbol{x}, \sigma) = 1\} \tag{12}$$

According to (12), the objective function value at $\boldsymbol{x}$ is the maximum variance σ for which the yield Y is still equal to one. This definition can be reformulated for other probability distributions (also determined by several coefficients) in a straightforward manner. The procedure for numerical evaluation of U_Y will be discussed in Section 2.3. A graphical illustration of the robustness enhancement process has been provided in Fig. 1.

2.2. Knowledge-Based Regression Surrogates by Response Features

In this work, in pursuit of computational efficiency, uncertainty quantification of the microwave component of interest is carried out using knowledge-based surrogate models constructed at the level of the response features. The response feature technique has been originally introduced to accelerate EM-driven optimization of high-frequency structures [47]. The key concept was to represent design objectives in terms of characteristic points of the system outputs (e.g., frequency/level coordinates of resonances, or frequencies corresponding to target levels of gain or axial ratio), i.e., the problem-specific knowledge extracted from the simulation data. A typically weakly nonlinear relationship between the feature points and geometry parameters, allows for achieving faster convergence of the optimization procedures [47], constructing surrogate models using smaller training data sets [53], but also obtaining quasi-global search capabilities using local algorithms [54].

For the purpose of robustness enhancement of microwave components, the definition of the feature points depends on the type of the circuit (coupler, filter, impedance transformer). Notwithstanding, we are either interested in points determining the system operating bandwidth at a specified level (e.g., –20 dB), or points determining the maximum/minimum in-band levels

of a chosen characteristic (e.g., return loss). Figure 2 shows the examples of feature point selection or a microwave coupler and a bandpass filter.

Information about the feature points will be gathered in a feature vector $\boldsymbol{P}$, which, at the design $\boldsymbol{x}$, is defined as

$$\boldsymbol{P}(\boldsymbol{x}) = [p_1(\boldsymbol{x})\ p_2(\boldsymbol{x}) \ldots\ p_{N_p}(\boldsymbol{x})]^T \tag{13}$$

where $p_k(\boldsymbol{x})$, $k = 1,\ldots, N_p$, are characteristic point coordinates (either frequencies or levels) pertinent to the design task at hand. The feature points are extracted from the EM-simulated circuit responses.

Let us consider two examples. In the case of a microwave coupler with design specifications formulated as in (1)-(3), we are primarily interested in the frequency coordinates of the points corresponding to –20 dB levels of matching and isolation response, $|S_{11}|$ and $|S_{41}|$, as well as the level coordinates of the transmission responses $|S_{21}|$ and $|S_{31}|$ at the intended operating frequencies. Consequently, for a single-band coupler, the feature vector takes the form of

$$\boldsymbol{P}(\boldsymbol{x}) = [p_1(\boldsymbol{x})\ p_2(\boldsymbol{x}) \ldots\ p_6(\boldsymbol{x})]^T = [f_1(\boldsymbol{x})\ f_2(\boldsymbol{x})\ f_3(\boldsymbol{x})\ f_4(\boldsymbol{x})\ l_1(\boldsymbol{x})\ l_2(\boldsymbol{x})]^T \tag{14}$$

where f_1 and f_2 are the frequencies corresponding to $S_{\max}$ (e.g., –20 dB) level of the matching response $|S_{11}|$, f_3 and f_4 are the frequencies corresponding to $S_{\max}$ level of the isolation response $|S_{41}|$, whereas l_1 and l_2 are the levels of $|S_{21}|$ and $|S_{31}|$, respectively, at the target operating frequency of the coupler (cf. Fig. 2(a)). For an N-band coupler, the corresponding feature vector takes the form of

$$\begin{aligned}\boldsymbol{P}(\boldsymbol{x}) &= [p_1(\boldsymbol{x})\ p_2(\boldsymbol{x}) \ldots\ p_{6N}(\boldsymbol{x})]^T = \\ &[f_{1.1}(\boldsymbol{x})\ f_{2.1}(\boldsymbol{x})\ f_{3.1}(\boldsymbol{x})\ f_{4.1}(\boldsymbol{x})\ l_{1.1}(\boldsymbol{x})\ l_{2.1}(\boldsymbol{x})\ \ldots\ f_{1.N}(\boldsymbol{x})\ f_{2.N}(\boldsymbol{x})\ f_{3.N}(\boldsymbol{x})\ f_{4.N}(\boldsymbol{x})\ l_{1.N}(\boldsymbol{x})\ l_{2.N}(\boldsymbol{x})]^T\end{aligned} \tag{15}$$

In (15), the second subscript indicates the operating band (from 1 to N). The design specifications (1)-(3) formulated for the multi-band coupler in Section 2.1 can now be expressed in terms of the response features as

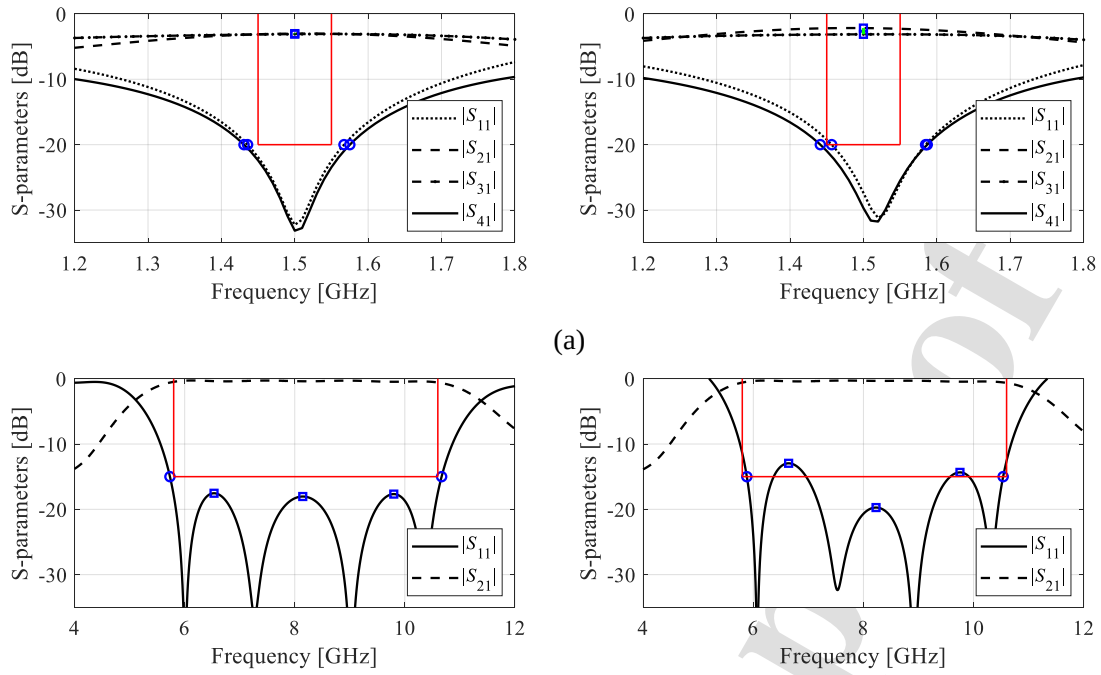

Fig. 2. Response features for exemplary microwave components: (a) scattering parameters of a coupler along with the response features corresponding to –20 dB level of matching ($|S_{11}|$) and isolation ($|S_{41}|$) characteristics (o), and transmission ($|S_{21}|$, $|S_{31}|$) at the target operating frequency of 1.5 GHz (□); the feature points allow for determining satisfaction of the performance requirements (here, the matching/isolation bandwidth of 1.45 GHz to 1.55 GHz, and maximum power split error of 0.5 dB at 1.5 GHz); (b) scattering parameters of a filter with the feature points corresponding to –15 dB level of $|S_{11}|$ and local maxima of $|S_{11}|$ within the filter operating band; the feature points permit determination of whether the return loss characteristic satisfies the matching conditions over the upper UWB bandwidth (5.9 GHz to 10.6 GHz). The left- and right-hand-side panels illustrate designs satisfying and violating the performance specifications, respectively.

$$f_{1.k}(\boldsymbol{x}) \le f_{L.k}, \quad f_{3.k}(\boldsymbol{x}) \le f_{L.k}, \quad k = 1, \ldots, N \tag{16}$$

$$f_{2.k}(\boldsymbol{x}) \ge f_{R.k}, \quad f_{4.k}(\boldsymbol{x}) \ge f_{R.k}, \quad k = 1, \ldots, N \tag{17}$$

$$|\, l_{1.k}(\boldsymbol{x}) - l_{2.k}(\boldsymbol{x}) \,| \le D_k, \quad k = 1, \ldots, N \tag{18}$$

As a second example, let us consider a *N*th-order bandpass filter with performance requirements formulated for the return loss characteristic using (4) (Section 2.1). In this case the feature vector will take the form of

$$\boldsymbol{P}(\boldsymbol{x}) = [\, p_1(\boldsymbol{x}) \; p_2(\boldsymbol{x}) \ldots p_{N+1}(\boldsymbol{x}) \,]^T = [\, f_1(\boldsymbol{x}) \; f_2(\boldsymbol{x}) \; l_1(\boldsymbol{x}) \; \ldots \; l_{N-1}(\boldsymbol{x}) \,]^T \tag{19}$$

where f_1 and f_2 are the frequencies corresponding to $S_{\max}$ (e.g., –20 dB level of $|S_{11}|$, and l_k, k = 1,…, N – 1, are the reflection levels corresponding to local in-band maxima of $|S_{11}|$ (note that

the filter should be well tuned in order for all maxima to be present, which is normally the case at the nominal design), cf. Fig. 2(b). Using (19), the design specifications (4) for the filter can be expressed as

$$f_1(\boldsymbol{x}) \le f_L, \quad f_2(\boldsymbol{x}) \ge f_R \tag{20}$$

$$l_k(\boldsymbol{x}) \le S_{\max}, \quad k = 1, \ldots, N-1 \tag{21}$$

The primary advantage of employing the response features is the aforementioned low sensitivity of feature point coordinates to geometry parameter variations. This property makes it possible to use simple (e.g., linear) surrogates that still have a sufficient predictive power in the neighborhood of the nominal design. From the point of view of robustness enhancement, this will translate into improved computational efficiency of the optimization process.

The robustness enhancement algorithm proposed in this work is an iterative procedure (cf. Section 2.4), with the feature-based surrogate model $\boldsymbol{L}_P^{(i)}(\boldsymbol{x})$ established at the current design point $\boldsymbol{x}^{(i)}$. The model represents the feature vector $\boldsymbol{P}$ and is defined as

$$\boldsymbol{L}_P^{(i)}(\boldsymbol{x}) = [\, p_{L.1}(\boldsymbol{x}) \ldots p_{L.N_p}(\boldsymbol{x})]^T = \begin{bmatrix} l_{0.1} + \boldsymbol{L}_1^T(\boldsymbol{x} - \boldsymbol{x}^{(i)}) \\ \vdots \\ l_{0.N_p} + \boldsymbol{L}_{2N_p}^T(\boldsymbol{x} - \boldsymbol{x}^{(i)}) \end{bmatrix} \tag{22}$$

The model coefficients are found as

$$\begin{bmatrix} l_{0.j} \\ \boldsymbol{L}_j \end{bmatrix} = \begin{bmatrix} 1 & (\boldsymbol{x}_B^{(1)} - \boldsymbol{x}^{(i)})^T \\ & \vdots \\ 1 & (\boldsymbol{x}_B^{(n+1)} - \boldsymbol{x}^{(i)})^T \end{bmatrix}^{-1} \begin{bmatrix} p_j(\boldsymbol{x}_B^{(1)}) \\ \vdots \\ p_j(\boldsymbol{x}_B^{(n+1)}) \end{bmatrix}, \quad j = 1, \ldots, N_p \tag{23}$$

where $\boldsymbol{x}_B^{(k)}$, $k = 1, \ldots, n+1$, are the training points, and $p_j(\boldsymbol{x}_B^{(k)})$ are the elements of the feature vectors $\boldsymbol{P}(\boldsymbol{x}_B^{(k)})$ extracted from EM-simulated circuit responses. The training vectors are allocated as $\boldsymbol{x}_B^{(1)} = \boldsymbol{x}^{(i)}$, and $\boldsymbol{x}_B^{(k)} = \boldsymbol{x}^{(i)} + [0 \ \ldots \ 0 \ d \ 0 \ \ldots \ 0]^T$ with d on the $(k-1)$th position. Here, we set $d = 3\sigma$, i.e., the parameter perturbations d correspond to the maximum deviation values.

2.3. Objective Function Evaluation

An important aspect of the robustness enhancement procedure discussed in this work is the evaluation of the objective function $U_Y(\boldsymbol{x})$ defined in (12). Here, it is carried out by numerical integration of the probability density function $p(\cdot)$ in (8), using—for the sake of expediting the process—the feature-based surrogate (22). More specifically, the model $\boldsymbol{L}_P^{(i)}(\boldsymbol{x})$, utilized throughout the ith iteration of the optimization algorithm, is employed as a predictor providing estimated values of the feature vector at the design $\boldsymbol{x}$, which, permits rapid verification of the design specifications (e.g., (16)-(18) in the case of a coupler, or (21), (22) in the case of a filter). The estimation of the yield $Y(\boldsymbol{x},\sigma)$ is realized using a large number of random observables $\boldsymbol{x}_r^{(j)}$ (here, N_r = 100,000) allocated using the assumed probability distribution governed by the variance σ. The following procedure is applied:

1. For a given variance σ, generate the observable set $\{\boldsymbol{x}_r^{(j)}\}_{j = 1, \ldots, Nr}$;
2. Evaluate the regression surrogate $\boldsymbol{L}_P^{(i)}(\boldsymbol{x}_r^{(j)})$ for $j = 1, \ldots, N_r$;
3. Evaluate design specifications (e.g., conditions (16)-(18), or (21), (22) for all $\boldsymbol{x}_r^{(j)}$ using surrogate-predicted features $p_{L.k}(\boldsymbol{x}_r^{(j)})$, $j = 1, \ldots, N_r$;
4. Compute $Y(\boldsymbol{x},\sigma)$ according to (9).

All steps of the above procedure are vectorized to speed up yield estimation, which allows for handling a large number of observables at a negligible cost. At the same time, involving large data sets considerably reduces the yield estimation variance.

The objective function $U_Y(\boldsymbol{x})$ is calculated by solving the problem (12). Here, we use a golden ratio search [55] because the probability distribution controlling the fabrication tolerances is parameterized by a single coefficient (the variance σ). In more complex situations, e.g., joint normal distributions governed by a given covariance matrix, other methods can be applied (e.g., gradient-based procedures). To distinguish the objective functions evaluated

using different feature-based surrogates, we introduce the symbol $U_Y^{(i)}(\boldsymbol{x})$ to denote the function associated to the model $\boldsymbol{L}_P^{(i)}$.

2.4. Complete Robustness Enhancement Algorithm

In order to exploit the feature-based surrogate and to ensure convergence of the robustness enhancement process, the problem (11) is solved iteratively using the trust-region (TR) framework [56]. The design $\boldsymbol{x}^{(i+1)}$ approximating $\boldsymbol{x}^*$ and produced in the ith iteration of the algorithm ($\boldsymbol{x}^{(0)}$ is the nominal design), is obtained as

$$\boldsymbol{x}^{(i+1)} = \arg\min_{\|\boldsymbol{x}-\boldsymbol{x}^{(i)}\|\le d^{(i)}} U_Y^{(i)}(\boldsymbol{x}) \tag{24}$$

The objective function $U_Y^{(i)}(\boldsymbol{x})$ in (24) is evaluated as described in Section 2.3. Note that the optimization process is constrained to the vicinity of the current design, defined as $\|\boldsymbol{x} - \boldsymbol{x}^{(i)}\| \le \delta^{(i)}$; the TR size is adjusted based on the gain ratio [56]

$$r = \frac{U_Y^{\#(i)}(\boldsymbol{x}^{(i+1)}) - U_Y^{(i)}(\boldsymbol{x}^{(i)})}{U_Y^{(i)}(\boldsymbol{x}^{(i+1)}) - U_Y^{(i)}(\boldsymbol{x}^{(i)})} \tag{25}$$

The denominator of (25) is the objective function improvement as predicted using the regression model. The numerator is calculated using $U_Y^{\#(i)}$, which is defined as in Section 2.3 but using the feature-based model $\boldsymbol{L}_P^{\#(i)}$, in which the coefficient vector $[l_{0.1} \ldots l_{0.Np}]^T$ is replaced by the feature point $\boldsymbol{P}(\boldsymbol{x}^{(i+1)})$, extracted from EM simulation data at $\boldsymbol{x}^{(i+1)}$.

Utilization of the model $U_Y^{\#(i)}$ allows for a computationally cheap validation of the design $\boldsymbol{x}^{(i+1)}$ (only one EM analysis is involved). The reliability of this validation is subject to the feature point gradients not changing rapidly between $\boldsymbol{x}^{(i)}$ and $\boldsymbol{x}^{(i+1)}$. This is normally justified by the very nature of the feature point relations with geometry parameters as well as small expected design relocations between the algorithm iterations. In particular, $\|\boldsymbol{x}^{(i+1)} - \boldsymbol{x}^{(i)}\|$ is typically comparable to the fraction of the variance σ.

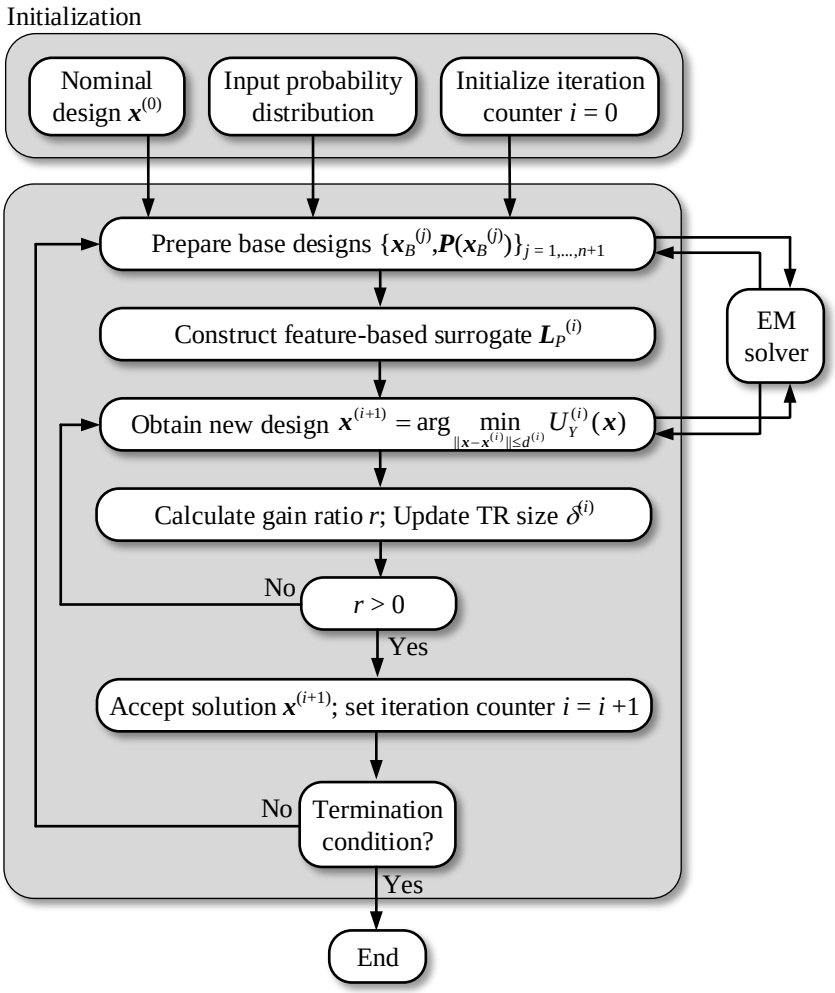

Fig. 3. Flow diagram of the robustness enhancement algorithm involving feature-based surrogates.

The vector $\boldsymbol{x}^{(i+1)}$ produced by (25) is accepted if the gain ratio $r > 0$, and it is rejected otherwise. In the latter case, the iteration is repeated with reduced $d^{(i)}$. The termination condition utilized in this work is $\|\boldsymbol{x}^{(i+1)} - \boldsymbol{x}^{(i)}\| < \varepsilon$ (convergence in argument) OR $\delta^{(i)} < \varepsilon$ (reducing the TR radius), with $\varepsilon = 10^{-3}$. Figure 3 shows the flow diagram of the proposed procedure.

3. Demonstration Case Studies

In this section, the tolerance optimization methodology introduced in Section 2 is demonstrated using three microstrip circuits, including two broadband filters and a compact branch line coupler. Given the performance requirements, the design goal is to enlarge the maximum input parameter deviations for which the perfect (100-percent) fabrication yield can

still be achieved. The reliability of the optimization process is corroborated through EM-driven Monte Carlo simulations at the nominal and the optimized designs.

3.1. Case Studies

For the sake of validation, we use the following three circuits:

- An upper UWB-band (5.8 GHz to 10.6 GHz) microstrip filter using a stepped-impedance resonator (SIR) [57], shown in Fig. 4(a) (Circuit I);
- A compact wideband filter using shunt resonators coupled through admittance inverters [58], shown in Fig. 4(b) (Circuit II);
- A miniaturized branch-line coupler (BLC) [58], shown in Fig. 4(c) (Circuit III).

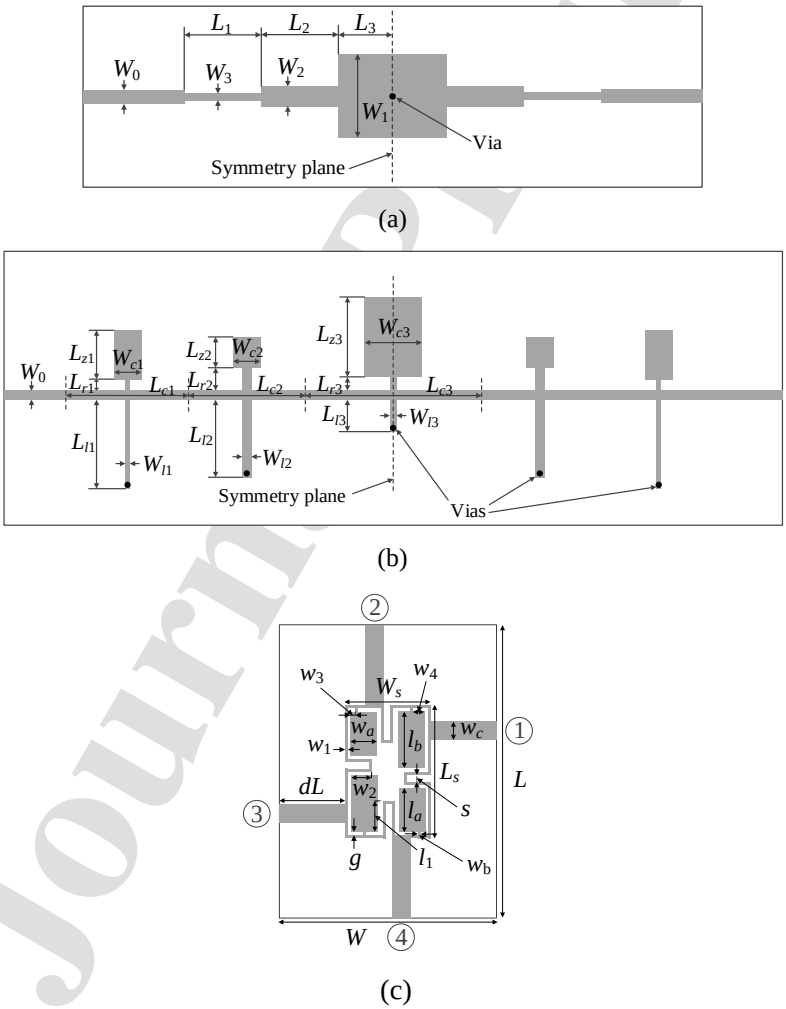

Fig. 4. Microwave circuits utilized for demonstrating the tolerance optimization procedure of Section 2: (a) UWB filter using stepped-impedance resonator (Circuit I) [57], (b) wideband filter using shunt resonators (Circuit II) [58], (c) miniaturized branch-line coupler (Circuit III) [59].

Table 2. Verification case studies

	Case study[$]		
	Circuit I	Circuit II	Circuit III
Substrate	RO4003C (ε_r = 3.55, h = 0.305 mm)	RO3010 (ε_r = 10.2, h = 0.63 mm)	AD300 (ε_r = 2.97, h = 0.76 mm)
Design parameters	$\boldsymbol{x} = [L_1\ L_2\ L_3\ W_1\ W_2\ W_3]^T$	$\boldsymbol{x} = [L_{l1}\ L_{l2}\ L_{l3}\ L_{c1}\ L_{c2}\ L_{c3}\ L_{r1}\ L_{r2}\ L_{r3}\ L_{z1}\ L_{z2}\ L_{z3}]^T$	$\boldsymbol{x} = [g\ l_{1r}\ l_a\ l_b\ w_1\ w_{2r}\ w_{3r}\ w_{4r}\ w_a\ w_b]^T$
Other parameters	W_0 = 0.66 mm	W_0 = 0.6 mm, $W_{c1} = W_{c2}$ = 2 mm, W_{c3} = 3 mm, $W_{l1} = W_{l3}$ = 0.3 mm, W_{l2} = 0.5 mm	$L = 2dL + L_s$, $L_s = 4w_1 + 4g$ + s + $l_a + l_b$, $W = 2dL + W_s$, $W_s = 4w_1 + 4g + s + 2w_a$, $l_1 = l_b l_{1r}$, $w_2 = w_a w_{2r}$, $w_3 = w_{3r} w_a$, and $w_4 = w_{4r} w_a$, w_c = 1.9 mm
Performance specifications	$\lvert S_{11}\rvert \leq -15$ dB within the operating band of 5.8 GHz to 10.6 GHz	$\lvert S_{11}\rvert \leq -15$ dB within the operating band of 2.1 GHz to 2.9 GHz	$\lvert S_{11}\rvert$, $\lvert S_{41}\rvert \leq -20$ dB within the operating band of 1.45 GHz – 1.55 GHz Power split $\lvert S_{21}\rvert - \lvert S_{31}\rvert \leq 0.5$ dB at 1.5 GHz
Nominal design	$\boldsymbol{x}^{(0)} = [4.25\ 5.20\ 4.04\ 6.69\ 1.07\ 0.47]^T$	$\boldsymbol{x}^{(0)} = [2.86\ 3.53\ 1.77\ 10.55\ 11.62\ 10.82\ 0.74\ 2.42\ 0.54\ 3.67\ 2.30\ 3.89]^T$	$\boldsymbol{x}^{(0)} = [0.63\ 5.90\ 9.34\ 12.45\ 1.29\ 2.02\ 0.99\ 0.32\ 2.81\ 0.22]^T$

[$] Parameters with subscript r are relative, and their deviations are recalculated accordingly in order to have the corresponding absolute parameters following the assumed probability distribution.

Table 2 provides the necessary data on the considered structures, including the material parameters of the dielectric substrate, geometry parameters, nominal design, as well as design specifications. The computational models of all circuits are evaluated using the time-domain solver of CST Microwave Studio [60] (software package for simulation of EM components and systems). All the simulations were performed on Intel Xeon 2.1 GHz dual-core CPU with 128 GB RAM.

The input (manufacturing) tolerances are represented by means of independent normal distributions with zero mean and a common variance σ. Further, the maximum parameter deviations are limited to 3σ. It should be noted that some of the circuit parameters are relative, in which case, their parameter deviations are recalculated (scaled) to comply with the assumed input tolerances for the corresponding absolute parameters (based on the functional dependencies provided in Table 2).

As mentioned before, the variance σ is the major evaluation metric, which is subject to maximization in the tolerance optimization process. Larger variance (for which the perfect, i.e.,

100-percent fabrication yield is still ensured) corresponds to higher levels of acceptable parameter deviations. The assumption of joint variance for independent Gaussian distributions, taken in this section, is reasonable due to the fact that most of geometry parameters are determined by the same fabrication process (e.g., chemical etching). At the same time, this can be generalized to, e.g., arbitrary covariance matrix that describes the relationships between the parameters. In that case, tolerance optimization procedure would be only different in a part pertinent to evaluation of the objective function U_Y, as mentioned in Section 2.3.

3.2. Results and Discussion

Table 3 gathers the numerical results, in particular, the variance and maximum parameter deviation ensuring 100-percent yield at the nominal design and after applying the robustness enhancement procedure. The obtained final designs for the considered circuits are:

- Circuit I: $\boldsymbol{x}^* = [4.24\ 5.17\ 4.02\ 6.71\ 1.06\ 0.47]^T$;
- Circuit II: $\boldsymbol{x}^* = [2.84\ 3.53\ 1.77\ 10.53\ 11.62\ 10.81\ 0.74\ 2.40\ 0.53\ 3.67\ 2.30\ 3.88]^T$;
- Circuit III: $\boldsymbol{x}^* = [0.64\ 5.90\ 9.27\ 12.51\ 1.27\ 2.01\ 1.06\ 0.33\ 2.85\ 0.22]^T$.

Table 3. Robustness enhancement results for the Circuit I, II, and III

Verification structure		Circuit I	Circuit II	Circuit III
Nominal design	Maximum variance σ ensuring 100-percent yield[@]	5.6 μm	1.2 μm	4.3 μm
	Maximum parameter deviation ensuring 100-percent yield	16.7 μm	3.7 μm	13.0 μm
	EM-based yield estimation[#]	100 %	98 %	100 %
Tolerance-optimized design	Maximum variance σ ensuring 100-percent yield[@]	8.7 μm	1.8 μm	7.7 μm
	Maximum parameter deviation ensuring 100-percent yield	26.1 μm	5.4 μm	23.0 μm
	EM-based yield estimation[#]	100 %	99 %	100 %
Optimization cost[$]		40	118	52

[@] σ refers to the variance of the independent zero-mean Gaussian distributions assumed to describe the fabrication tolerances. The maximum parameter deviations are assumed to be 3σ.
[#] Estimation obtained using Monte Carlo simulation based on 500 random samples.
[$] Optimization cost in terms of the number of EM analyses of the circuit under design.

It should be noted that the CPU cost of finding the robust designs is low. It corresponds to just 40, 118, and 52 EM simulations of the respective circuits. Although the cost for Circuit II is considerably higher than for other structures, the dimensionality of the parameters is also higher (12 parameters versus six for Circuit I and ten for Circuit III). The primary factor enabling computational speedup is utilization of feature-based surrogates, which permits rapid uncertainty quantification.

The design relocations are generally small, which is due to the fact that the responses of all circuits are highly dependent of their geometry parameters. Nevertheless, the proposed robustness enhancement procedure allows for a considerable increase of the input tolerance levels ensuring 100-percent fabrication yield, by a factor of 1.6, 1.5, and 1.8 for Circuit I, II, and III. In absolute terms, the maximum parameter deviations increase from 16.7 μm to 26.1 μm (Circuit I), from 3.7 μm to 5.4 μm (Circuit II), and from 13.0 μm to 23.0 μm (Circuit III). The average improvement ratio factor exceeds 1.6.

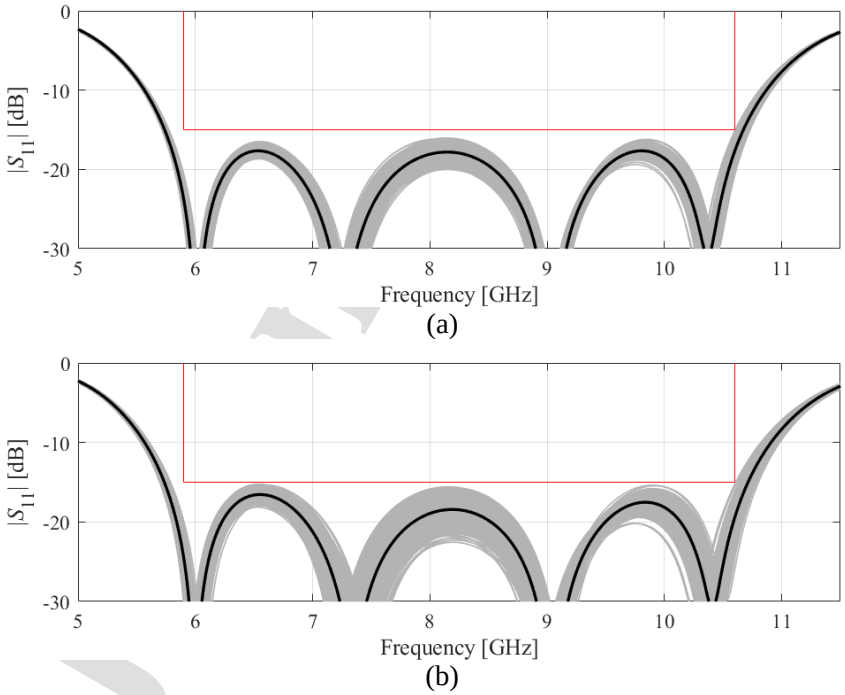

Fig. 5. EM-driven Monte Carlo analysis of Circuit I (Fig. 4(a)) at (a) the nominal design, and (b) the design found using the robustness enhancement algorithm. Black plots indicate the circuit responses at the nominal and the optimized designs, respectively, gray plots represent EM simulation data at the random observables generated during the MC analysis.

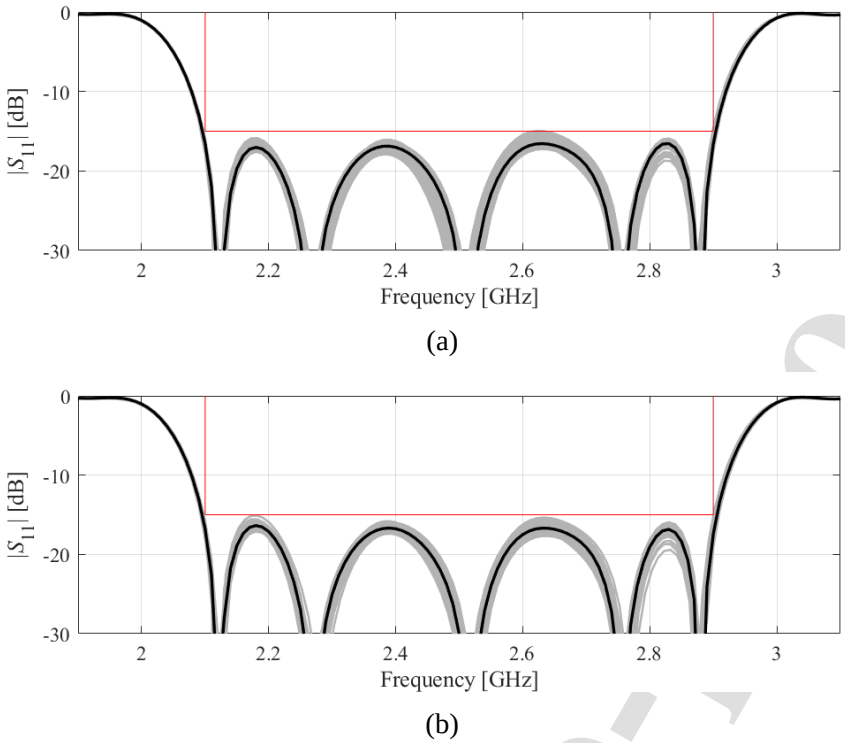

Fig. 6. EM-driven Monte Carlo analysis of Circuit II (Fig. 4(b)) at (a) the nominal design, and (b) the design found using the robustness enhancement algorithm. Black plots indicate the circuit responses at the nominal and the optimized designs, respectively, gray plots represent EM simulation data at the random observables generated during the MC analysis.

For the sake of reliability, EM-based Monte Carlo analysis using 500 random samples has been executed for both the nominal and the robust design. The purpose was to verify whether 100-percent yield is indeed preserved, which would be a confirmation of a sufficient predictive power of the feature-based surrogates utilized for uncertainty quantification. It can be observed (Table 3) that the MC-validated yield is 100 percent for Circuit I and Circuit II, and it is slightly lower for Circuit II. It should be emphasized that EM-driven MC exhibits relatively large standard deviation of yield estimation, which is inversely proportional to $N_r^{1/2}$; at the same time, the number of samples was limited to 500 due to the high CPU cost of the procedure.

Graphical illustrations of MC can be found in Figs. 5 through 7. It can be observed that the allowable tolerance levels are much higher at the optimized designs than at the nominal ones, which is indicated by the broader spread of the circuit characteristics (grey plots). The

improvement obtained by relocating the design manifests itself by slight broadening of the bandwidth at the expense of other characteristics (e.g., the increase of the in-band maxima for the filter structures). Also, in all cases, the families of circuit responses are essentially touching the specification lines, which is a visual confirmation of both the fact that the yield at both the nominal and the robust design is close to 100 percent, and that the tolerance levels cannot be improved further.

Let us compare the proposed robustness enhancement technique with conventional approaches: simulation-based and surrogate-assisted procedures. The cost of the former (i.e., direct EM-driven tolerance-aware design using e.g., Monte Carlo simulation) is in most cases tremendous and may reach up few thousand EM analyses. The employment of surrogate-based frameworks may somewhat alleviate this issue, still, they are not free from shortcomings.

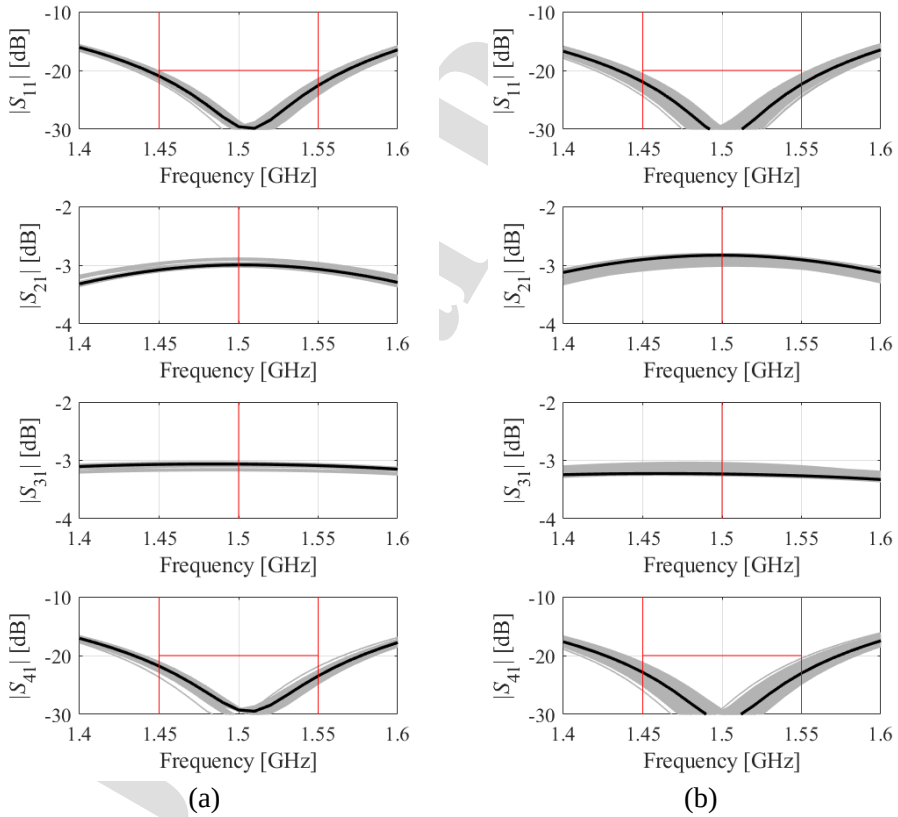

Fig. 7. EM-driven Monte Carlo analysis of Circuit III (Fig. 4(c)) at (a) the nominal design, and (b) the design found using the robustness enhancement algorithm. Black plots indicate the circuit responses at the nominal and the optimized designs, respectively, gray plots represent EM simulation data at the random observables generated during the MC analysis.

In fact, traditional surrogate modeling techniques are to a large extent limited in terms of design space dimensionality and the ranges of geometry parameters due to the observed highly nonlinear characteristics of microwave components. This severely hinders their applicability to the devices described by low numbers of design variables, which is far from sufficient. Whereas our approach allows for performing the robustness improvement task cost-efficiently, and, at the same time does not impose any limitations on the parameter space dimensionality. As a matter of fact, the structures utilized in this work as verification case studies are quite challenging ones, as they are described by six, ten and twelve geometry parameters. Finally, it should be mentioned, that most of statistical design procedures described in the high-frequency design literature (cf. Section 1) are oriented towards yield maximization, whereas there are almost no works that directly tackle tolerance improvement in the sense considered in this work. This is yet another advantage of the proposed approach, because—instead of finding the designs that improve the fabrication yield as much as possible—it directly maximizes acceptable levels of parameter deviations. This information can be used, among others, to select the manufacturing process that ensures perfect fabrication yield.

4. Conclusion

This work presented a novel procedure for accelerated robustness enhancement of microwave components under uncertainties. The objective is to maximize the permitted levels of geometry parameter deviations, for which the perfect (100-percent) fabrication yield can be ensured. The primary benefit of this formulation is that it allows for explicit prediction data on input tolerances, thereby facilitating a selection of a suitable manufacturing process or meaningful comparison of alternative circuit topologies for a given application. The key components of the proposed procedure are knowledge-based surrogates set up at the level of the response features, a vectorized implementation of Monte Carlo integration of probability density functions determining the tolerances, as well as embedding the optimization process in

the trust region framework to secure its convergence. Comprehensive verification experiments have been carried out using three microstrip circuits, including two broadband filters and a compact branch-line coupler. A significant improvement of the input tolerance levels has been achieved in all cases, by a (multiplication) factor of 1.6 on the average. Despite relatively large dimensionalities of the corresponding parameter spaces (six, twelve, and ten variables), the average CPU cost of the robustness enhancement process is merely seventy EM analyses of the respective circuits. Due to its efficacy and easy implementation, the methodology introduced in this paper may be an attractive tool of choice for reliable and expedited EM-driven robust design of microwave components.

The major findings are that incorporating knowledge-based surrogates constructed at the level of the feature points allows for obtaining a considerable improvement of the input tolerance levels (nearly twofold on the average) at low computational cost. Achieving this may be primarily attributed to exploitation of the problem-specific knowledge in the form of the response features embedded in the acquired data. In addition, the employment of feature-based surrogates for yield estimation dramatically reduces computational expenditures, whereas executing iterative search with the use of the trust-region routine guarantees its convergence. The scope of applicability of the proposed technique is limited to the components of responses featuring easily discernible characteristic points. Notwithstanding, because tolerance optimization typically requires reasonably small relocation of the parameter vector, the existence of response features is generally not an issue. Also, in many cases, the frequency characteristics of real-world microwave passives are inherently well-structured (e.g., couplers, multi-band transformers or power dividers). Consequently, the techniques formulated at the level of the response features may be successfully employed for the structures of these classes. The future work will be aimed at increasing its

versatility of the proposed technique to other types of high-frequency components (e.g., antennas of various types of responses such as multi-band or wideband).

Acknowledgment

The authors would like to thank Dassault Systemes, France, for making CST Microwave Studio available. This work was supported in part by the Icelandic Centre for Research (RANNIS) Grant 217771, and by National Science Centre of Poland Grant 2018/31/B/ST7/02369.

References

[1] D. Parveg, M. Varonen, D. Karaca, and K. Halonen, "Wideband mm-wave CMOS slow wave coupler," *IEEE Microwave Wireless Comp. Lett.*, vol. 29, no. 3, pp. 210-212, 2019.

[2] E. Musonda, R. A. Paradkar, I. C. Hunter, and R. Parry, "Synthesis of multiband filters by linear optimization," *IEEE Trans. Microwave Theory Techn.*, vol. 67, no. 12, pp. 4764-4772, 2019.

[3] H. Xu, Y. Wang, F. A. Ghaffar, and L. Roy, "Reconfigurable microwave filters implemented using field programmable microwave substrate," *IEEE Trans. Microwave Theory Techn.*, vol. 69, no. 2, pp. 1344-1354, 2021.

[4] M. Ali, F. Liu, A. Watanabe, P.M. Raj, V. Sundaram, and M.M. Tentzeris, "First demonstration of compact, ultra-thin low-pass and bandpass filters for 5G small-cell applications," *IEEE Microwave Wireless Comp. Lett.*, vol. 28, no. 12, pp. 1110-1112, 2018.

[5] Y. Wang, J. Zhang, F. Peng, and S. Wu, "A glasses frame antenna for the applications in internet of things," *IEEE Internet of Things J.*, vol. 6, no. 5, pp. 8911-8918, 2019.

[6] H. Ahn, M. M. Tentzeris, T. Lin, B. Tehrani, and X. He, "Coupled lines for wearable power dividers: coupled transmission-line sections for power dividers in wearable and flexible RF electronics," *IEEE Microwave Mag.*, vol. 21, no. 2, pp. 66-87, 2020.

[7] J. -G. Chi and Y. -J. Kim, "A compact wideband millimeter-wave quadrature hybrid coupler using artificial transmission lines on a glass substrate," *IEEE Microwave Wireless Comp. Lett.*, vol. 30, no. 11, pp. 1037-1040, 2020.

[8] X. Tan, J. Sun, and F. Lin, "A compact frequency-reconfigurable rat-race coupler," *IEEE Microwave Wireless Comp. Lett.*, vol. 30, no. 7, pp. 665-668, 2020.

[9] Q. Li and T. Yang, "Compact UWB half-mode SIW bandpass filter with fully reconfigurable single and dual notched bands," *IEEE Trans. Microwave Theory Techn.*, vol. 69, no. 1, pp. 65-74, 2021.

[10] A. Sieganschin, B. Tegowski, T. Jaschke, and A. F. Jacob, "Compact diplexers with folded circular SIW cavity filters," *IEEE Trans. Microwave Theory Techn.*, vol. 69, no. 1, pp. 111-118, 2021.

[11] L.M.Q. Abualigah, *Feature Selection and Enhanced Krill Herd Algorithm for Text Document Clustering*, Springer, New York, 2019.

[12] L. Abualigah, A. Diabat, S. Mirjalili, M. A., A. H. Gandomi, "The arithmetic optimization algorithm," *Comp. Methods Applied Mech. Eng.*, vol. 376, art. no. 113609, 2021.

[13] L. Abualigah, D. Yousri, M. A. Elaziz, A. A. Ewees, M. A.A. Al-qaness, A. H. Gandomi, "Aquila Optimizer: A novel meta-heuristic optimization algorithm," *Computers Industrial Eng.*, vol. 157, art. no. 107250, 2021.

[14] R. Biernacki, S. Chen, G. Estep, J. Rousset, and J. Sifri, "Statistical analysis and yield optimization in practical RF and microwave systems," *IEEE MTT-S Int. Microw. Symp. Dig.*, Montreal, pp. 1-3, 2012.

[15] A.S.O. Hassan and A.S.A. Mohamed, "Surrogate-based circuit design centering" In: Koziel S, Leifsson L. (Eds.) *Surrogate-based modeling and Optimization*, pp. 27–49, Springer, NY, 2013.

[16] Q. Wu, W. Chen, C. Yu, H. Wang, and W. Hong, "Multilayer machine learning-assisted optimization-based robust design and its applications to antennas and arrays," *IEEE Trans. Ant. Prop.*, Early view, 2021.

[17] A. Singhee and R. A. Rutenbar, "Why quasi-Monte Carlo is better than Monte Carlo or Latin sampling for statistical circuit analysis," *IEEE Trans. Computer-Aided Design of Integrated Circuits Syst.*, vol. 29, no. 11, pp. 1763-1776, 2010.

[18] H. Ahn and S. Nam, "Compact microstrip 3-dB coupled-line ring and branch-line hybrids with new symmetric equivalent circuits," *IEEE Trans. Microwave Theory Techn.*, vol. 61, no. 3, pp. 1067-1078, 2013.

[19] M. Sengupta, S. Saxena, L. Daldoss, G. Kramer, S. Minehane, and J. Cheng, "Application-specific worst case corners using response surfaces and statistical models," *IEEE Trans. Comput.-Aided Design Integr. Circuits Syst.*, vol. 24, no. 9, pp. 1372–1380, 2005.

[20] B. Zhang and Y. Rahmat-Samii, "Robust optimization with worst case sensitivity analysis applied to array synthesis and antenna designs," *IEEE Trans. Ant. Propag.*, vol. 66, no. 1, pp. 160–171, 2018.

[21] J.E. Rayas-Sanchez, V. Gutierrez-Ayala, "EM-based statistical analysis and yield estimation using linear-input and neural-output space mapping," *IEEE MTT-S Int. Microwave Symp. Digest (IMS)*, pp. 1597-1600, 2006.

[22] A. K. Prasad and S. Roy, "Reduced dimensional chebyshev-polynomial chaos approach for fast mixed epistemic-aleatory uncertainty quantification of transmission line

networks," *IEEE Trans. Comp. Packaging Manufacturing Techn.*, vol. 9, no. 6, pp. 1119-1132, 2019.

[23] S. Koziel and A. Pietrenko-Dabrowska, "Recent advances in high-frequency modeling by means of domain confinement and nested kriging," *IEEE Access*, vol. 8, pp. 189326-189342, 2020.

[24] J. Jin, C. Zhang, F. Feng, W. Na, J. Ma, and Q. Zhang, "Deep neural network technique for high-dimensional microwave modeling and applications to parameter extraction of microwave filters," *IEEE Trans. Microwave Theory Techn.*, vol. 67, no. 10, pp. 4140-4155, 2019.

[25] B. Liu, H. Yang, and M. J. Lancaster, "Global optimization of microwave filters based on a surrogate model-assisted evolutionary algorithm," *IEEE Trans. Microwave Theory Techn.*, vol. 65, no. 6, pp. 1976-1985, 2017.

[26] J. Du and C. Roblin, "Statistical modeling of disturbed antennas based on the polynomial chaos expansion," *IEEE Ant. Wireless Prop. Lett.*, vol. 16, p. 1843-1847, 2017.

[27] P. Kersaudy, S. Mostarshedi, B. Sudret, O. Picon, and J. Wiart, "Stochastic analysis of scattered field by building facades using polynomial chaos," *IEEE Trans. Ant. Propag.*, vol. 62, no. 12, pp. 6382-6393, 2014.

[28] H.L. Abdel-Malek, A.S.O. Hassan, E.A. Soliman, and S.A. Dakroury, "The ellipsoidal technique for design centering of microwave circuits exploiting space-mapping interpolating surrogates," *IEEE Trans. Microwave Theory Techn.*, vol. 54, no. 10, pp. 3731-3738, 2006.

[29] L. Leifsson, X. Du, and S. Koziel, "Efficient yield estimation of multi-band patch antennas by polynomial chaos-based kriging," *Int. J. Numerical Modeling*, vol. 33, no. 6, e2722, 2020.

[30] J.S. Ochoa and A.C. Cangellaris, "Random-space dimensionality reduction for expedient yield estimation of passive microwave structures," *IEEE Trans. Microwave Theory Techn.*, vol. 61, no. 12, pp. 4313-4321, 2013.

[31] D. Spina, F. Ferranti, G. Antonini, T. Dhaene, and L. Knockaert, "Efficient variability analysis of electromagnetic systems via polynomial chaos and model order reduction," *IEEE Trans. Comp. Packaging Manufacturing Techn.*, vol. 4, no. 6, pp. 1038-1051, 2014.

[32] M.C. Kennedy and A. O'Hagan, "Predicting the output from complex computer code when fast approximations are available", *Biometrika*, vol. 87, pp. 1-13, 2000.

[33] J.P. Jacobs and S. Koziel, "Reduced-cost microwave filter modeling using a two-stage Gaussian process regression approach," *Int. J. RF and Microwave CAE*, vol. 25, no. 5, pp. 453-462, 2014.

[34] J. Zhang, F. Feng, J. Jin, and Q.-J. Zhang, "Efficient yield estimation of microwave structures using mesh deformation-incorporated space mapping surrogates," *IEEE Microwave Wireless Comp. Lett.*, vol. 30, no. 10, pp. 937-940, 2020.

[35] A. Pietrenko-Dabrowska, S. Koziel, and M. Al-Hasan, „Expedited yield optimization of narrow- and multi-band antennas using performance-driven surrogates," *IEEE Access*, pp. 143104-143113, 2020.

[36] A. Pietrenko-Dabrowska, "Rapid tolerance-aware design of miniaturized microwave passives by means of confined-domain surrogates," *Int. J. Numerical Modeling*, vol. 33, no. 6, e2779, 2021.

[37] Y. Li, Y. Ding, and E. Zio, "Random fuzzy extension of the universal generating function approach for the reliability assessment of multi-state systems under aleatory and epistemic uncertainties," *IEEE Trans. Reliability*, vol. 63, no. 1, pp. 13-25, 2014.

[38] G. J. K. Tomy and K. J. Vinoy, "A fast polynomial chaos expansion for uncertainty quantification in stochastic electromagnetic problems," *IEEE Ant. Wireless Propag. Lett.*, vol. 18, no. 10, pp. 2120-2124, 2019.

[39] A.S.O. Hassan, H.L. Abdel-Malek, A.S.A. Mohamed, T.M. Abuelfadl, and A.E. Elqenawy, "Statistical design centering of RF cavity linear accelerator via non-derivative trust region optimization," *IEEE Int. Conf. Numerical EM Multiphysics Modeling Opt. (NEMO)*, pp. 1-3, 2015.

[40] G. Scotti, P. Tommasino, and A. Trifiletti, "MMIC yield optimization by design centering and off-chip controllers," *IET Proceedings - Circuits, Devices and Systems*, vol. 152, no. 1, pp. 54-60, Feb. 2005.

[41] H. Acikgoz and R. Mittra, "Stochastic polynomial chaos expansion analysis of a split-ring resonator at terahertz frequencies," *IEEE Trans. Ant. Propag.*, vol. 66, no. 4, pp. 2131-2134, 2018.

[42] A. Kouassi, N. Nguyen-Trong, T. Kaufmann, S. Lallechere, P. Bonnet, and C. Fumeaux, "Reliability-aware optimization of a wideband antenna," *IEEE Trans. Ant. Prop.*, vol. 64, no. 2, pp. 450-460, 2016.

[43] J. Zhang, C. Zhang, F. Feng, W. Zhang, J. Ma, and Q.J. Zhang, "Polynomial chaos-based approach to yield-driven EM optimization," *IEEE Trans. Microwave Theory Tech.*, vol. 66, no. 7, pp. 3186-3199, 2018.

[44] Q. Wu, W. Chen, H. Wang, and W. Hong, "Machine learning-assisted tolerance analysis and its application to antennas," *IEEE Int. Symp. Ant. Propag.*, pp. 1853-1854, Montreal, Canada, 2020.

[45] H.M. Torun and M. Swaminathan, "High-dimensional global optimization method for high-frequency electronic design," *IEEE Trans. Microwave Theory Techn.*, vol. 67, no. 6, pp. 2128-2142, 2019.

[46] S. Koziel and A. Bekasiewicz, "Sequential approximate optimization for statistical analysis and yield optimization of circularly polarized antennas," *IET Microwaves Ant. Prop.*, vol. 12, no. 13, pp. 2060-2064, 2018.

[47] S. Koziel, "Fast simulation-driven antenna design using response-feature surrogates," *Int. J. RF & Microwave CAE*, vol. 25, no. 5, pp. 394-402, 2015.

[48] S. Koziel and J.W. Bandler, "Reliable microwave modeling by means of variable-fidelity response features," *IEEE Trans. Microwave Theory Tech.*, vol. 63, no. 12, pp. 4247-4254, 2015.

[49] S. Koziel and A. Pietrenko-Dabrowska, *Performance-driven surrogate modeling of high-frequency structures*, Springer, New York, 2020.

[50] A. Hardock, H. Brüns, and C. Schuster, "Chebyshev filter design using vias as quasi-transmission lines in printed circuit boards," *IEEE Trans. Microwave Theory Tech.*, vol. 63, no. 3, pp. 976-985, 2015.

[51] M.A. Haq and S. Koziel, "On topology modifications for wideband antenna miniaturization," *AEU - Int. J. Electr. Comm.*, vol. 94, pp. 215-220, 2018.

[52] D. Kim, M. Kim, and W. Kim, "Wafer edge yield prediction using a combined long short-term memory and feed- forward neural network model for semiconductor manufacturing," *IEEE Access*, vol. 8, pp. 215125-215132, 2020.

[53] A. Pietrenko-Dabrowska and S. Koziel, "Simulation-driven antenna modeling by means of response features and confined domains of reduced dimensionality," *IEEE Access*, vol. 8, pp. 228942-228954, 2020.

[54] S. Koziel and A. Pietrenko-Dabrowska, "Expedited feature-based quasi-global optimization of multi-band antennas with Jacobian variability tracking," *IEEE Access*, vol. 8, pp. 83907-83915, 2020.

[55] W.H. Press, S.A. Teukolsky, W.T. Vetterling, and B.P. Flannery, "Golden section search in one dimension," in *Numerical Recipes: The Art of Scientific Computing* (3rd ed.), Cambridge University Press, New York, 2007.

[56] A.R. Conn, N.I.M. Gould, and P.L. Toint, *Trust Region Methods*, MPS-SIAM Series on Optimization, 2000.

[57] M. Zukocinski, "A 5.8-10.6 GHz UWB filter using novel SIR structure," *Int. Microwave Radar Conf. (MIKON)*, Poznan, Poland, 14-17 May, 2018.

[58] M. Sans, J. Selga, A. Rodríguez, J. Bonache, V. E. Boria, and F. Martín, "Design of planar wideband bandpass filters from specifications using a two-step aggressive space mapping (ASM) optimization algorithm," *IEEE Trans. Microwave Theory Tech.*, vol. 62, no. 12, pp. 3341-3350, 2014.

[59] L. Xia, J. Li, B. A. Twumasi, P. Liu, and S. Gao, "Planar dual-band branch-line coupler with large frequency ratio," *IEEE Access*, vol. 8, pp. 33188-33195, 2020.

[60] CST Microwave Studio, Dassault Systemes, Vélizy-Villacoublay, France, 2018.